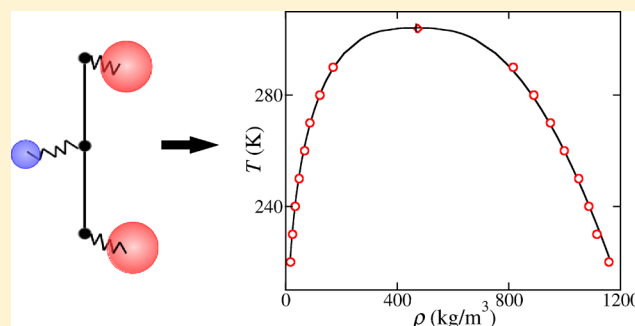


Gaussian-Charge Polarizable and Nonpolarizable Models for CO₂Hao Jiang,[†] Othonas A. Moulton,[‡] Ioannis G. Economou,[‡] and Athanassios Z. Panagiotopoulos^{*,†}[†]Department of Chemical and Biological Engineering, Princeton University, Princeton, New Jersey 08544, United States[‡]Chemical Engineering Program, Texas A&M University at Qatar, P.O. Box 23874, Doha, Qatar

S Supporting Information

ABSTRACT: A polarizable intermolecular potential model using three classical Drude oscillators on the atomic sites has been developed for CO₂. The model is rigid with bond lengths and molecular geometries set to their experimental values. Electrostatic interactions are represented by three Gaussian charges connected to the molecular frame by harmonic springs. Nonelectrostatic interactions are represented by the Buckingham exponential-6 potential, with potential parameters optimized to vapor–liquid equilibria (VLE) data. A nonpolarizable CO₂ model that shares the other ingredients of the polarizable model was also developed and optimized to VLE data. Gibbs ensemble Monte Carlo and molecular dynamics simulations were used to evaluate the two models with respect to a variety of thermodynamic and transport properties, including the enthalpy of vaporization, second virial coefficient, density in the one-phase fluid region, isobaric and isochoric heat capacities, radial distribution functions, self-diffusion coefficient, and shear viscosity. Excellent agreement between model predictions and experimental data was found for all properties studied. The polarizable and nonpolarizable models provide a similar representation of CO₂ properties, which indicates that the properties of pure CO₂ fluid are not strongly affected by polarization. The polarizable model, which has an order of magnitude higher computational cost than the nonpolarizable model, will likely be useful for the study of a mixture of CO₂ and polar components for which polarization is important.



I. INTRODUCTION

CO₂ is the most important greenhouse gas leading to global warming.¹ There are increasing needs for accurate modeling of its thermodynamic properties for many chemical processes, especially in connection to CO₂ capture. The sequestration of CO₂ in underground geologic formations, primarily saline aquifers, is a promising way to reduce the emission of CO₂.² Under the pressure and temperature conditions of geological CO₂ storage, prediction of thermophysical properties for the CO₂ + H₂O (or brine) mixture is extremely challenging for classical thermodynamic models, such as equations of state and activity coefficient models. Molecular modeling and simulation provide predictive alternative paths to obtain thermodynamic and transport properties of complex fluid mixtures.^{3–5} With an accurate molecular model, a large variety of thermophysical properties under a wide range of conditions can be obtained with high accuracy using molecular simulation techniques.

There have been several classical, nonpolarizable intermolecular potential models for CO₂. Murthy et al.⁶ developed two- and three-site models with Lennard-Jones (LJ) interactions that included a point quadrupole moment placed at the molecule center of mass. Möller⁷ and Fischer developed a model with two LJ interaction sites plus a point quadrupole, with parameters fitted to vapor–liquid equilibrium (VLE) data. Later, Vrabec et al.⁸ reparametrized the model of ref 7 to obtain a better representation of VLE. The “elementary physical models” (EPM and EPM2), developed by Harris and Yung,⁹

are the most widely used models for CO₂. These models have three LJ interaction sites with point charges located on the centers of each atom. The point charges of the EPM and EPM2 models were chosen to reproduce the gas-phase quadrupole moment. For the EPM model, the LJ parameters were chosen to reproduce the internal energy and pressure at 239 K, while the EPM2 model was rescaled from the EPM model to reproduce the critical properties. Another widely used CO₂ model is the TraPPE model, which was developed by Potoff and Siepmann.¹⁰ The TraPPE model was optimized to the VLE of the CO₂ and propane mixture. An exponential-6 (exp-6) model with point charges was developed by Potoff et al.,¹¹ with parameters also fitted to VLE data. Zhang and Duan proposed a model utilizing three LJ sites with point charges and claimed to achieve an accuracy of 0.7% for saturated vapor pressure.¹² However, Merker et al.¹³ found a deviation of 18% from experimental data for the vapor pressure using the model of ref 12. Merker et al.¹⁴ reported a model with three LJ sites plus point quadrupole, and claimed that the point quadrupole can be represented by three point charges. The model was optimized to VLE data, and the deviations between model and experiment were reported to be 0.4% in saturated liquid density and 1.8% in vapor pressure, which is quite remarkable

Received: November 30, 2015

Revised: January 15, 2016

Published: January 20, 2016

for any molecular model. Persson developed a “One-Center Anisotropic plus Quadrupole” model for CO₂, with model parameters fitted to VLE data.¹⁵ The model is computationally efficient, but significantly underestimates the second virial coefficient and does not represent well the CO₂ liquid structure (radial distribution function). While all these models were directly fitted to bulk experimental data, *ab initio* methods were also used to develop potential models for CO₂. An intermolecular potential with 5 interaction sites and complex interaction potentials was parametrized by Bock et al.¹⁶ with *ab initio* calculations. Bukowski et al.¹⁷ proposed an intermolecular potential for CO₂ from symmetry-adapted perturbation theory. Bratschi et al. concluded that the VLE behavior is generally not very accurately represented by these *ab initio*-based models.¹⁸

CO₂ is a linear and symmetric molecule with a zero dipole moment, which suggests that the electric field at long distances from a CO₂ molecule is negligible. Therefore, even though CO₂ is quite polarizable, the effects of polarizability on the thermophysical properties of pure CO₂ are not expected to be significant, and CO₂ models without polarizability are able to achieve good accuracy in the prediction of the pure component properties. However, when mixed with a polar component, such as water, the mixture properties may not be accurately predicted by nonpolarizable models. Vlcek et al.¹⁹ optimized unlike-pair interactions for a CO₂–H₂O mixture using SPC/E and EPM2 models; however, the compositions of the CO₂-rich phase at 348 K are not properly represented. Recently, Orozco et al.²⁰ conducted Gibbs ensemble MC simulations to study the VLE of the CO₂–H₂O mixture. It was found that nonpolarizable models, such as TraPPE model,¹⁰ have limitations in the prediction of compositions and densities for both vapor and liquid phases. Introducing polarizability into potential models may be a promising way to improve model performance for mixture of CO₂ with H₂O or other polar components.

There are two sets of polarizable CO₂ models available in the literature. Persson²¹ proposed a Gaussian-charge polarizable (GCP) interaction potential for CO₂. This model has an induced dipole, plus an Axilrod-Teller correction term²² for dispersion interactions, and gives satisfactory results for the second and third virial coefficients. However, VLE and other important macroscopic properties of the GCP CO₂ model were not reported, possibly due to the computational difficulties of the model. Yu et al.²³ developed a physically motivated, *ab initio* model for CO₂, namely, the SYM model. In the SYM model, polarization of the CO₂ molecule is reproduced using a shell model (or Drude oscillator model), in which positive point charges (core) are located at the nucleus and negative point charges (shell) are attached to each polarizable atoms. Positive (core) and negative (shell) charges are connected by a harmonic spring, and the positions of the negative shell charges are optimized at each simulation step. This model yields good representations of many macroscopic properties, including VLE, fluid phase density, isobaric heat capacity, and diffusion coefficient. It is noticed that the Thole screening function²⁴ should be applied in this model to avoid the polarization catastrophe caused by the short distance between polarizable sites. In addition, a total of six charges were used in this model, which significantly increases the computation cost compared to a three-site CO₂ model.

Recently, a Drude oscillator-based polarizable H₂O model (BK3) that uses Gaussian charge and Buckingham exp-6 potential was developed by Kiss and Baranyai.²⁵ Over the entire phase diagram, the BK3 water model gives satisfactory

estimates for many properties, including density, vapor pressure, viscosity, and so on. The BK3 water and ion models²⁶ were also found to accurately predict the thermodynamic and transport properties of binary H₂O + NaCl mixture;²⁷ hence, we believe the BK3-style polarizable models form a good basis for the development of a comprehensive molecular model for CO₂ sequestration calculations. In this work, we aim to design, in the same spirit, Drude oscillator-based polarizable and nonpolarizable CO₂ models that are able to give accurate representation of many thermophysical properties for pure CO₂ and which can be easily combined with other BK3-style polarizable models to study complex fluid mixtures. Specifically, given the success of the BK3 model for pure water, we believe it is promising for accurate representation of thermodynamic and transport properties of the binary H₂O + CO₂ mixture, which is of great importance to the design of CO₂ geological storage.

The paper is structured as follows: the new Gaussian charge Drude oscillator polarizable CO₂ model and the Gaussian charge nonpolarizable CO₂ model are presented in section II, and the simulation details are described in section III. The performance of these new models with respect to the calculation or prediction of VLE, second virial coefficient, density in one-phase fluid region, isobaric and isochoric heat capacities, structure, diffusion coefficient, and shear viscosity are given in section IV. Finally, the main conclusions are summarized in section V.

II. MODEL

The structure of the CO₂ molecule is well-known from experiment: it has a linear geometry with a C–O bond length of 1.162 Å.²⁸ Since the internal (vibrational) degrees of freedom do not have a significant effect on the VLE, which is our primary interest, we chose to use a rigid and linear geometry for both the polarizable and nonpolarizable models and used the experiment C–O distance²⁸ as the bond length of our models.

The electrostatic interaction of CO₂ is modeled by Gaussian charges, instead of the more commonly used point charges. The use of Gaussian charges for molecular models, was pioneered by Chialvo and Cummings.²⁹ It involves a spherical charge distribution of the form

$$\rho_i = \frac{q_i}{(2\pi\sigma_i^2)^{3/2}} \exp\left(\frac{-|r - r_i|^2}{2\sigma_i^2}\right) \quad (1)$$

where ρ_i is the charge density and σ_i is the width of charge distribution. The Coulomb energy of two interacting Gaussian charges (i, j) is given as²⁵

$$U_{\text{coul}} = \frac{q_i q_j}{4\pi\epsilon_0 |r_i - r_j|} \operatorname{erf}\left(\frac{|r_i - r_j|}{\sqrt{2(\sigma_i^2 + \sigma_j^2)}}\right) \quad (2)$$

Kiss et al.³⁰ showed that with efficient handling for the real-space part of Ewald summation, the computational cost of Gaussian charges is only 10% higher than point charges, while the numerical stability of the model is significantly improved by using Gaussian charges. The distribution of the Gaussian charges in our proposed polarizable model is similar to the previously published point charge CO₂ models: without the influence of external electric field, the center of the positive charge rests on the carbon atom, and centers of two negative charges rest on the oxygen atoms. The magnitude of the

positive charge is $+0.6595e$, determined by matching the experiment quadrupole moment (-4.278 D \AA).³¹ It was found that the properties of pure CO_2 fluid were not strongly dependent on the widths of Gaussian charges, however, the choice of Gaussian charge width was not completely arbitrary. With a small width parameter ($<0.3 \text{ \AA}$), Gaussian charge behaves similar to the point charge and the model is numerically less stable. Under the influence of a strong external electric field, energy minimization of Drude particles, which has to be performed at each simulation step, becomes computationally expensive because a small iteration step size must be used to avoid the polarization catastrophe. On the other hand, having a very large width parameter is also not desirable. When the Gaussian charge width is large ($>1 \text{ \AA}$) and comparable with the Ewald screening length, the Ewald summation of Gaussian charges³² in real space converges slowly and one may need to either increase the cutoff distance or number of wave vectors, which increases the computational cost. Hence, to have a model that is stable and computationally efficient, we set the width parameters to 0.9 \AA for negative charges. For positive charge, the width parameter was arbitrarily set to 0.5 \AA since its effects on simulation efficiency and model results are not pronounced.

In general, there are three approaches to model polarizability: fluctuating charges, polarizable dipoles or multipoles, and Drude oscillators. Although the fluctuating charge approach is computationally efficient, the polarizability of the model tends to be constrained on the molecular plane. For polarizable dipoles, the evaluation of induced dipole interactions are complex and generally not supported by currently available molecular simulation packages. In this work, we chose to use the Drude oscillator (or charge-on-spring) approach, so as to avoid the evaluation of long-range interactions between point dipoles. Chialvo et al.³³ showed recently that the polarizable Gaussian dipole approach is essentially equivalent to the Drude oscillator approach. In the Drude oscillator approach, a partial charge is attached to a fixed point on the molecular frame by a harmonic spring with a zero equilibrium length. If an external electric field is applied to the molecule, the harmonic spring elongates until the spring force balances the Coulomb force. From the equality of spring force and Coulomb force, the spring constant is determined as $k_s = q^2/\alpha$ (α is the polarizability). The polarization energy is the energy stored on the harmonic spring. In the present polarizable CO_2 model, the center of positive charge is connected to the carbon atom with harmonic spring, while the centers of negative charges are linked with oxygen atoms with harmonic springs. We used the experimental polarizability of CO_2 , 2.507 \AA^3 ,³⁴ and distributed it evenly to all the three charges (Drude particles) in the model. Since the polarization was modeled with three isotropic Drude oscillators, the molecular polarizability tensor of CO_2 cannot be accurately represented by the proposed model. As previously observed for the BK3 H_2O model,²⁵ we were able to use only three charge sites to describe the three-dimensional polarization of CO_2 molecule, without any damping function, because of the excellent numerical stability resulting from the Gaussian charges. Since the primary computational cost for the simulation of a polarizable model lies in the energy minimization of Drude particles instead of the Ewald summation for electrostatic interactions, one may argue that it is desirable to assign charges on molecular frame and have a six-site model, such as the polarizable SYM model by Yu et al.,²³ which is able to use stiffer springs (shell particles with higher charge magnitude) and, consequently, reduce the

number of iterations needed for the energy minimization. However, it was found that for simulations using the proposed three-site model, the energy minimization generally converged within three iterations, and it was about 2 times faster than simulations using a six-site model. Therefore, compared to the polarizable SYM model,²³ which uses six charge sites and a Thole screening function,²⁴ our model is more computationally efficient. A schematic of the proposed model is shown in Figure 1.

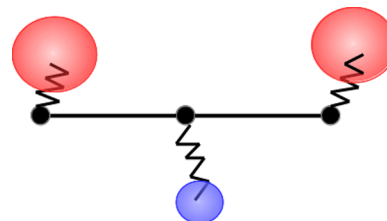


Figure 1. Schematic representation of the polarizable CO_2 model. The polarization of the CO_2 molecule is three-dimensional.

For the nonpolarizable model, the partial Gaussian charges are located on the center of carbon and oxygen atoms, and there is no need to perform energy minimization during a simulation since the positions of charges are fixed on the molecular frame.

The van der Waals interaction is represented by the Buckingham exp-6 potential,

$$U_{\text{vdW}} = A \exp(-Br) - C/r^6 \quad (3)$$

where r is the distance between two interaction sites. The exponential term is believed to be more realistic than the r^{-12} term in description of repulsive interaction between adjacent molecules.²⁵ In addition, the exp-6 potential with three adjustable parameters provides more flexibility for parameter optimization than the commonly used two-parameter LJ potential. For the cross interaction parameters A_{OC} and B_{OC} between carbon and oxygen, the Kong combining rules were used,³⁵

$$A_{\text{OC}} = \frac{1}{2} \left[A_{\text{O}} \left(\frac{A_{\text{O}}B_{\text{O}}}{A_{\text{C}}B_{\text{C}}} \right)^{-B_{\text{O}}/(B_{\text{O}}+B_{\text{C}})} + A_{\text{C}} \left(\frac{A_{\text{C}}B_{\text{C}}}{A_{\text{O}}B_{\text{O}}} \right)^{-B_{\text{C}}/(B_{\text{O}}+B_{\text{C}})} \right] \quad (4)$$

$$B_{\text{OC}} = \frac{2B_{\text{O}}B_{\text{C}}}{B_{\text{O}} + B_{\text{C}}} \quad (5)$$

while the “C” parameter was calculated using the geometric mixing rule.

Since our goal is to have a CO_2 model that is reliable for the study of thermodynamic and transport properties, especially for the VLE properties, we chose to adjust the model parameters to the VLE data of pure CO_2 fluid instead of any first-principle calculation results. We found that the VLE calculation is not sensitive to the choice of distribution of polarizability or Gaussian charge widths. Hence, only the exp-6 potential parameters (A , B , C) were fitted to the experimental saturated vapor pressures, saturated vapor and liquid densities from 220 to 290 K.³⁶ The second virial coefficient at 220 K, which is a gas phase property, is also included in the parameter optimization. The optimization method employed in this work was proposed by Ungerer et al.³⁷ and successfully applied by Eckl et al.³⁸ to

Table 1. Parameters of the Polarizable (Top) and Nonpolarizable (Bottom) CO₂ Models

atom	A (MJ/mol)	B (Å ⁻¹)	C (kJ/mol/Å ⁶)	q (e)	σ (Å)	α (Å ³)	geometry
C	78.29	3.55	728	0.660	0.500	0.836	<i>r</i> _{CO} = 1.162 Å
O	329.71	3.93	1548	-0.330	0.900	0.836	∠OCO = 180°
C	81.38	3.73	765	0.660	0.500		<i>r</i> _{CO} = 1.162 Å
O	357.87	3.93	1560	-0.330	0.900		∠OCO = 180°

design a molecular model for ammonia. This method is based on a least-squares minimization of a weighted objective function F ,

$$F = \frac{1}{n} \sum_{i=1}^n \frac{1}{\delta A_{\text{sim},i}} (A_{\text{sim},i}(\mathbf{P}) - A_{\text{expt},i}) \quad (6)$$

where \mathbf{P} is the vector of model parameters ($\mathbf{P} = [p_1, p_2, \dots, p_m]$), $A_{\text{sim},i}$ is the simulation result for property i and $A_{\text{expt},i}$ is the corresponding experimental value. The objective function F is weighted by the simulation uncertainty $\delta A_{\text{sim},i}$. The Gaussian-Newton algorithm was used to minimize the objective function F , and the partial derivative of the simulation property $A_{\text{sim},i}$ with respect to the model parameter p_j can be approximated by a finite difference scheme provided that the variation δp_j is not too large,

$$\frac{\delta A_{\text{sim},i}}{\delta p_j} = \frac{A_{\text{sim},i}(p_0, p_1, \dots, p_j + \delta p_j, \dots, p_m) - A_{\text{sim},i}(p_0, p_1, \dots, p_j, \dots, p_m)}{\delta p_j} \quad (7)$$

We first did several manual tweaks to find sets of parameters for both the polarizable and nonpolarizable models that gave reasonable representation of VLE for CO₂. With these sets of parameters as initial guesses, 8–10 Gaussian-Newton iterations were performed to obtain the final sets of parameters for both polarizable and nonpolarizable models. Further iterations or manual tweak of model parameters did not significantly change the representation of VLE properties or second virial coefficient, hence, we believe the resulting sets of parameters are indeed close to a local minimum of the objective function F . The final (optimized) model parameters are given in Table 1.

III. SIMULATION DETAILS

A. Gibbs Ensemble MC Simulations. The VLE properties, including saturated vapor pressure, saturated vapor and liquid density, and enthalpy of vaporization were obtained from Gibbs ensemble MC (GEMC) simulations at constant volume and temperature.^{39,40} Since the interactions of polarizable models are not pairwise additive, we used a multiparticle move method to efficiently sample phase space. The multiparticle move method was originally developed by Moučka et al.,⁴¹ and was successfully used to simulate polarizable H₂O + NaCl models.^{27,42} During the simulations, all CO₂ molecules in both vapor and liquid phases were translated or rotated simultaneously in one step. The base system size for simulations of the polarizable model was 256 CO₂ molecules, while 512 molecules were used in the simulation of nonpolarizable model. Finite-size effects were tested by doubling the system size at 220 and 280 K; vapor pressures and phase densities obtained were within statistical uncertainties of results obtained from the base system size. The cutoff distance for the Buckingham potential and real space Coulomb interactions were set to 9 Å for liquid phase box and 11 Å for vapor phase box, respectively. The standard long-range correction⁴³ was applied to the r^{-6} part of the Buckingham potential for both vapor and liquid phase boxes.

The long-range part of the Gaussian electrostatic interactions was handled by Ewald summation.^{32,44} The number of wave vectors for the Ewald summation was between 800 and 1000, achieving a relative accuracy of 10⁻⁴ in electrostatic energy. The forces on the Drude particles were calculated at every MC step, and the positions of Drude particles were calculated with the following iteration scheme,

$$\mathbf{r}_{\text{ID}}(n) = \mathbf{r}_{\text{ID}}(n-1) + \mathbf{F}_{\text{ID}}/k \quad (8)$$

where $\mathbf{r}_{\text{ID}}(n)$ denotes the position of Drude particle of molecule i in step n of the iteration, \mathbf{F}_{ID} is the force acting on the Drude particle, and k is the spring constant of the harmonic spring connecting the Drude particle. The iteration was terminated if the condition

$$\max_{i=1 \dots N} |\mathbf{r}_{\text{ID}}(n) - \mathbf{r}_{\text{ID}}(n-1)| < 10^{-4} \text{ nm} \quad (9)$$

was satisfied. For simulation of the nonpolarizable model, the standard single particle move⁴³ was performed and the above-mentioned iteration was not needed since the positions of charges are fixed with respect to the molecular frame.

For the polarizable CO₂ model, a typical GEMC simulation consisted of an equilibration period of 1 million steps, followed by a production period of 5 million steps. The MC moves were multiparticle translations (constituting a fraction of 0.15 of total moves), multiparticle rotations (0.15), volume changes (0.2), and transfers of particles with configurational bias (0.5).⁴⁵ The maximum displacements in the multiparticle translation and rotation moves were adjusted during the equilibration period of the simulation to achieve an average acceptance ratio of 30%. The volume change moves were performed isotropically in the standard fashion,⁴³ and the maximum volume change was also adjusted during the equilibration period to achieve 30% average acceptance. The acceptance ratio of transfer moves was between 3 and 18%, depending on the temperature. GEMC simulations were performed with the Cassandra suite of MC codes⁴⁶ with our in-house modifications to handle polarizable models. A typical GEMC simulation of polarizable CO₂ model took about 80 h using eight 2.6 GHz Intel Sandybridge cores. For the nonpolarizable CO₂ model, a typical GEMC simulation consisted of 100 million steps with first 20 million steps as equilibration period, and single particle translation and rotation moves were performed. Using Cassandra, a typical GEMC simulation of the nonpolarizable model took about 10 h to complete on four 2.6 GHz Intel Sandybridge cores.

The second virial coefficient (B_2) was calculated using the rotation and energy routines of the Cassandra code, and it was obtained by a numerical integration of Mayer function,

$$B_2(T) = -2\pi \int_0^\infty (\langle e^{-U/k_B T} \rangle - 1) r^2 dr \quad (10)$$

where the upper limit of the integration was set to 25 Å, beyond which the integrand is negligible. The average of Boltzmann factor was taken over 50000 randomly sampled molecular orientations at a fixed intermolecular distance.

B. Molecular Dynamics Simulations. The liquid density in the one-phase fluid region, isobaric and isochoric heat capacity, diffusion coefficient, viscosity and structure in terms of radial distribution functions were obtained from MD simulations in the isothermal–isobaric ensemble. Nosé-Hoover⁴⁷ thermostat and Parrinello-Rahman⁴⁸ barostat, with coupling constants of 0.5 and 1.0 ps, respectively, were used to control the system temperature and pressure. For the calculation of densities, the systems were equilibrated for 200 ps followed by a production period of 800 ps. For the calculation of heat capacities, the systems were equilibrated for 2 ns and a 8 ns production period was used to sample the fluctuation of total energy. The integration time step was set to 1 fs for both equilibration and production periods. The number of CO₂ molecules used in the MD simulations was 500, and the Buckingham interaction and real-space Gaussian electrostatics were cut at 15 Å. No system size effect was found for the calculation of density and heat capacity by performing a series of MD simulations with 864 CO₂ molecules. Standard pressure and energy correction was applied for the long-range part of the Buckingham potential, and the long-range Gaussian electrostatics were handled by the particle-mesh Ewald (PME) method proposed by Kiss et al.,³⁰ with a Fourier spacing parameter of 0.12 nm, which is the distance between grid points in PME method. The positions of the Drude particles were determined by the modified “Always Stable Predictor-Corrector” method of Kolafa,^{30,49} and the force on the Drude particle was relaxed to 0.05 kJ/(mol·nm). MD simulations were performed using the open-source GROMACS package,⁵⁰ modified by Kiss et al.³⁰ to include polarizable models.

Self-diffusion coefficients were calculated using the Einstein relation, according to which D is obtained from the solute mean square displacement:^{51,52}

$$D = \lim_{t \rightarrow \infty} \frac{\left\langle \frac{1}{N} \sum_{i=1}^N [r_i(t) - r_i(0)]^2 \right\rangle}{6t} \quad (11)$$

where $r_i(t)$ is the unfolded position of the center of mass of the molecule at time t , and the angle brackets indicate an ensemble average over all molecules and time origins. Each run had a 1 ns equilibration period followed by 10 ns production period. In order to improve statistics, the diffusion coefficient for each state point was calculated by averaging the results of 10 independent simulations, each one started from a different initial configuration. The molecular trajectories were sampled every 1000 steps, resulting in a total of 1000 configurations per run, from which diffusion coefficients were calculated. As reported in the literature, the long-range interactions in molecular dynamics simulations with periodic boundary conditions lead to significant system size effects on the diffusion coefficients.^{53–55} Prior work on CO₂⁵⁵ has shown that the diffusion coefficients depend inversely on simulation box size L . Thus, the diffusion coefficient at infinite system-size D^∞ can be obtained from the Yeh-Hummer relation:⁵³

$$D_{\text{MD}} = D^\infty - \frac{k_B T \xi}{6\pi\eta L} \quad (12)$$

where D_{MD} is the self-diffusion coefficient obtained from simulations, k_B is the Boltzmann constant, T is the absolute temperature, η is the viscosity, and $\xi \approx 2.837298$ is a dimensionless constant determined by an Ewald-like summation of a periodic lattice.⁵³ All diffusion coefficients reported in this work were corrected for system-size effects using eq 12.

The viscosity was calculated using the Green-Kubo relation:^{27,51}

$$\eta(t) = \frac{V}{k_B T} \int_0^t \langle P_{\alpha\beta}(t_0) P_{\alpha\beta}(t_0 + t) \rangle dt \quad (13)$$

where V is the volume of the simulation box and $P_{\alpha\beta}$ denotes the off-diagonal element of the pressure tensor. The angle brackets indicate an ensemble average over all time origins. In order to reduce statistical uncertainty, we averaged the autocorrelation functions over all independent off-diagonal tensor elements P_{xy} , P_{xz} , P_{yz} ; because of rotational invariance, we also added the equivalent $(P_{xx} - P_{yy})/2$ and $(P_{yy} - P_{zz})/2$ terms. Viscosity at each state point was calculated from three independent simulations. Each run was 10 ns long, while the pressure tensor elements were sampled every time step. The upper limit t of the integral in eq 13 was 6–8 ps.

IV. RESULTS AND DISCUSSION

Saturated vapor pressure, saturated vapor and liquid phase density, enthalpy of vaporization, second virial coefficient, density in homogeneous fluid region, isobaric and isochoric heat capacities, structure of CO₂ in terms of radial distribution function, diffusion coefficient and shear viscosity were calculated using the proposed models and methods described in the previous section. Numerical data and their associated simulation uncertainties are listed in [Supporting Information](#). Simulation uncertainties were estimated by dividing the production runs into 5–8 blocks and calculating the standard deviations of the block averages, or from multiple independent runs, as described in the previous section.

A. VLE Properties. Figure 2 shows the vapor–liquid coexistence curve of the polarizable and nonpolarizable proposed CO₂ models from 220 to 290 K. By adjusting the Buckingham potential parameters, simulation results are brought into excellent agreement with experimental data.³⁶

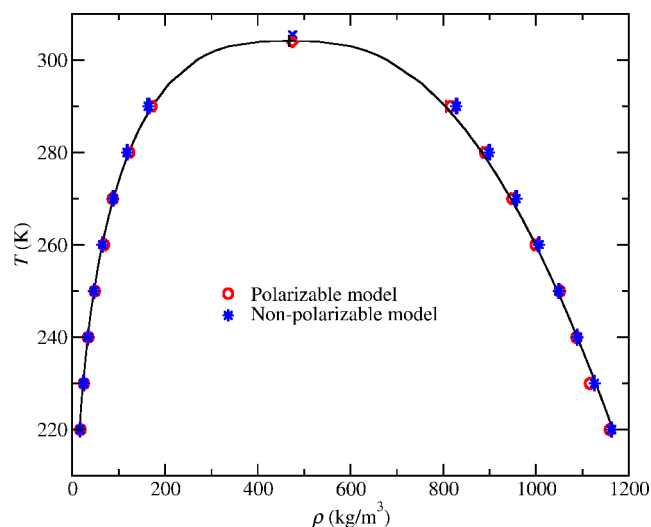


Figure 2. Vapor–liquid coexistence curve of the proposed polarizable and nonpolarizable CO₂ models from 220 to 290 K. Solid line is experimental data from NIST,³⁶ open circles are simulation results from the polarizable model and stars are simulation results from the nonpolarizable model. The experimental critical point is represented by “+”, the critical point of the polarizable model from extrapolation is represented by diamond and the critical point of the nonpolarizable model from extrapolation is represented by “X”.

For the polarizable model, the average relative deviations from experiment measurement are 0.6% for saturated liquid densities and 3.7% for saturated vapor densities, respectively. The relative deviation for the nonpolarizable model is 0.9% for saturated liquid densities and 2.4% for saturated vapor densities. When temperature is above 280 K, due to the small free energy difference between vapor and liquid phases, the GEMC simulation converged relatively slowly and the simulation uncertainties were more pronounced. Therefore, the highest temperature studied by the GEMC simulation was 290 K, and the critical points of the proposed models were obtained by extrapolating the density–temperature curve with the following equations:⁴³

$$\frac{\rho_L + \rho_V}{2} = \rho_c + a(T - T_c) \quad (14)$$

$$\rho_L - \rho_V = b(T - T_c)^{0.32} \quad (15)$$

where a and b are fitted parameters. The critical points estimated from the extrapolation are 303.9 K and 474.2 kg/m³ for the polarizable CO₂ model, and 305.5 K and 475.1 kg/m³ for the nonpolarizable model, which are in close agreement with experimental values³⁶ (304.13 K and 467.6 kg/m³, respectively).

Figure 3 shows the saturated vapor pressure calculated from the proposed CO₂ models. In general, the calculated saturated

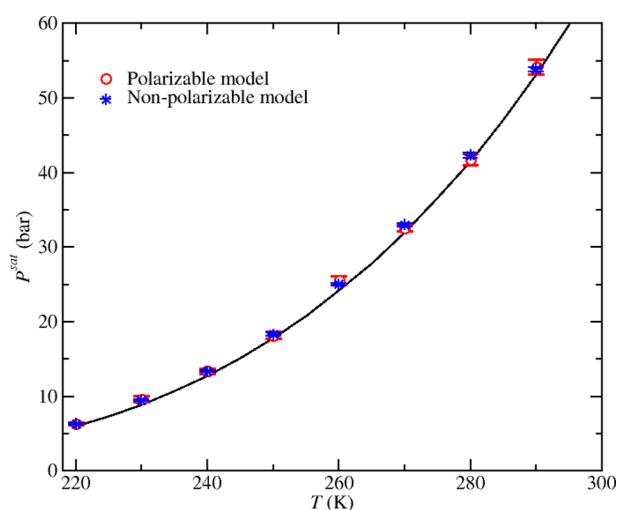


Figure 3. Saturated vapor pressure of the proposed polarizable and nonpolarizable CO₂ models from 220 to 290 K. Solid line is experimental data from NIST,³⁶ open circles are simulation results from the polarizable model and stars are simulation results from the nonpolarizable model.

vapor pressure is in good agreement with experimental data.³⁶ The average relative deviation from experiment is 3.7% and 2.4% for polarizable and nonpolarizable models, respectively, with both models slightly overestimating the vapor pressure. Figure 4 shows the enthalpy of vaporization calculated from the proposed CO₂ models. Although the enthalpy of vaporization data were not used in the parameter fitting, the simulation results for both polarizable and nonpolarizable models are in perfect agreement with experimental data, with average relative error smaller than 2.0%.

B. Second Virial Coefficient. The second virial coefficients (B_2) calculated from the proposed polarizable and non-

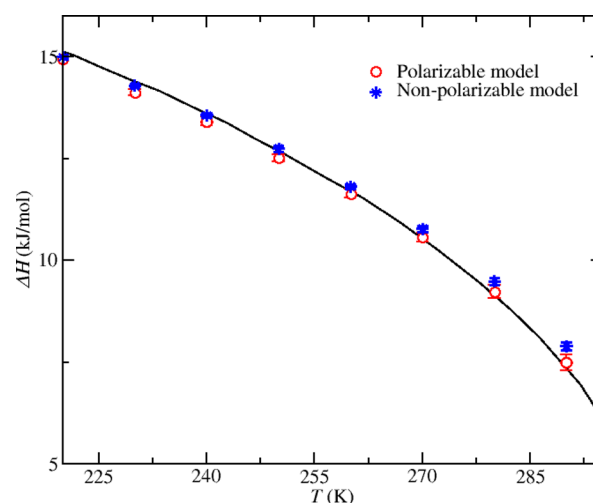


Figure 4. Enthalpy of vaporization of the proposed polarizable and nonpolarizable CO₂ models from 220 to 290 K. Solid line is experimental data from NIST,³⁶ open circles are simulation results from the polarizable model and stars are simulation results from the nonpolarizable model.

polarizable CO₂ models are compared with experimental data⁵⁶ in Figure 5. The polarizable and nonpolarizable models

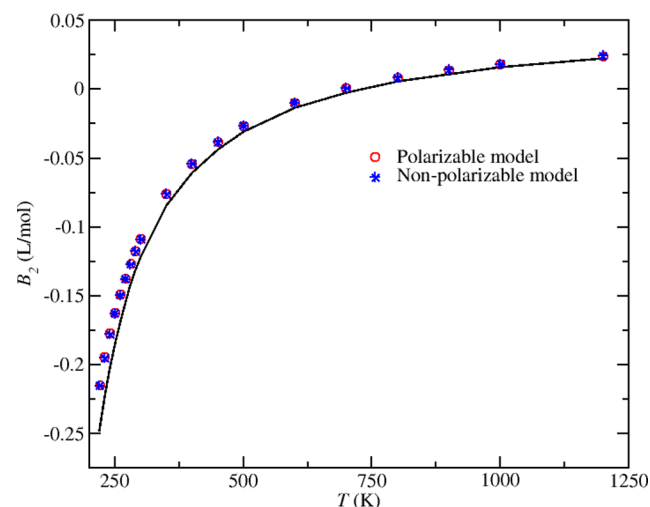


Figure 5. Second virial coefficients of the proposed polarizable and nonpolarizable CO₂ models from 220 to 1200 K. Solid line is experimental data,⁵⁶ open circles are simulation results from the polarizable model and stars are simulation results from the nonpolarizable model.

give very similar prediction of second virial coefficient, and both models exhibit reasonable agreement with experimental measurements. However, the calculated B_2 coefficients are systematically higher (less negative) than the experimental values, with larger deviations at low temperatures, despite the fact that B_2 at 220 K was included in the model parametrization. It was found that a small change of the exp-6 potential parameter (e.g., B parameter of oxygen in the polarizable model increases by 1%) can lead to a satisfactory representation of B_2 , but at the cost of poor representation of saturation density and pressure. This tradeoff between bulk properties and virial coefficients is believed to be caused by the missing three-body effects.²¹ Recently, Yu and Schmidt⁵⁷ demonstrated that three-

body interactions are essential to achieve excellent description for both second/third virial coefficient and bulk properties. Yu and Schmidt⁵⁷ found that the many-body effects of CO₂ model are mainly due to dispersion and exchange rather than polarization. Therefore, even though the many-body effects from polarization are accounted for in our models, these still overestimate B_2 at low temperatures.

C. Fluid Properties. Densities of CO₂ in the one-phase fluid region were calculated using the proposed polarizable and nonpolarizable models at various conditions and compared with experimental data from NIST.³⁶ As shown in Figure 6, the

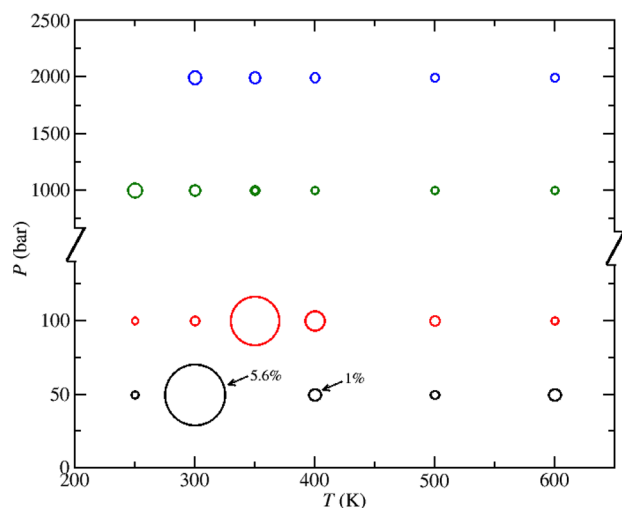


Figure 6. Relative deviations for density in one-phase fluid region between the polarizable model calculation and experimental data.³⁶ The size of circles is proportional to the relative deviation.

densities of CO₂ in fluid region are well predicted by the proposed polarizable model with typical relative error smaller than 1%. The fluid density predicted by the proposed nonpolarizable model is very similar to that obtained from the polarizable model, thus results for the nonpolarizable model are not shown in Figure 6 but given in Supporting Information. The largest deviation from experimental data,³⁶ which is 5.6% for the polarizable model and 4.9% for the nonpolarizable model, lies near the critical region. This is most likely due to the slight deviation of critical point, as shown in Figure 2.

Isobaric heat capacities (C_p) at $P = 100$ bar were calculated from the proposed models and shown in Figure 7. The intermolecular contribution to heat capacity was estimated from the enthalpy fluctuation in NPT-MD simulations. For a potential model with rigid geometry, the intramolecular contribution to heat capacity is not accessible by simulations, and can be approximated by the harmonic oscillator assumption,

$$C_p^{\text{intra}} = \sum_i \frac{(h\nu_i/k_B T)^2 e^{-h\nu_i/k_B T}}{(1 - e^{-h\nu_i/k_B T})^2} \quad (16)$$

where ν_i is the experimental CO₂ vibration frequency.⁵⁸ The summation runs over all 4 vibration modes of CO₂. At temperatures below 350 K, the intramolecular (vibrational) contributions to the isobaric heat capacity are generally less than 8%, while at temperatures above 400 K these contribute about 20–40%. With the intramolecular contribution calculated with eq 16, the proposed polarizable and nonpolarizable CO₂

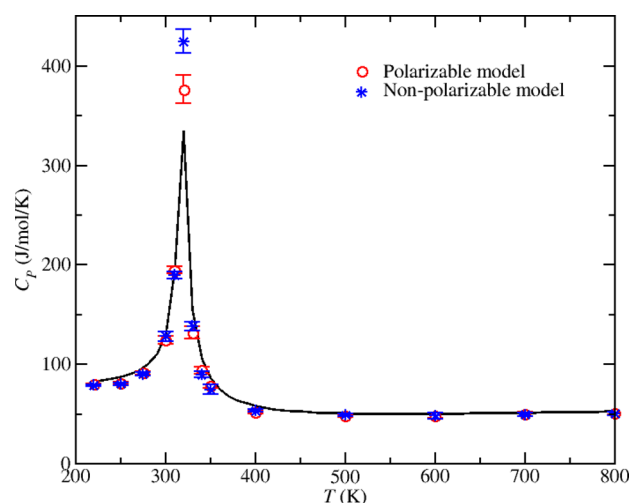


Figure 7. Isobaric heat capacity (C_p) of the polarizable and nonpolarizable CO₂ models. Solid line is experimental data from NIST,³⁶ open circles are simulation results from the polarizable model and stars are simulation results from the nonpolarizable model. The intramolecular contribution from eq 16 is included in the calculation.

models predict the isobaric heat capacities at 100 bar reasonably well. The C_p – T curve shows a peak around 320 K due to the dramatic change of system density in the critical region, and the proposed models successfully capture this critical behavior although the heat capacity near the critical point is overestimated by both the polarizable and nonpolarizable models. Figure 8 shows the isochoric heat capacity

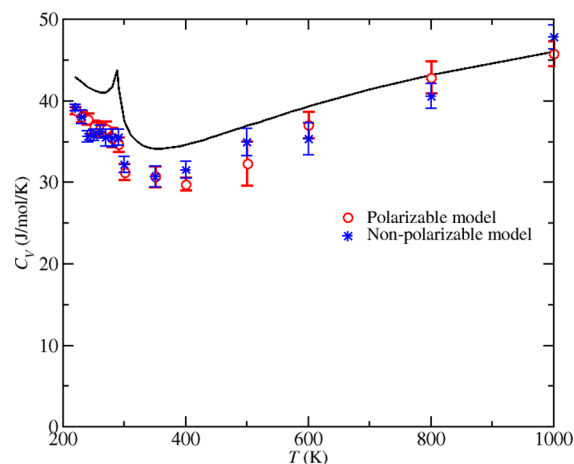


Figure 8. Isochoric heat capacity (C_V) of the polarizable and nonpolarizable CO₂ models. Solid line is experimental data from NIST,³⁶ open circles are simulation results from the polarizable model and stars are simulation results from the nonpolarizable model. The intramolecular contribution from eq 16 is included in the calculation.

(C_V) at 50 bar. Both the polarizable and nonpolarizable models give very similar prediction and follow the trend of experimental data, however, the isochoric heat capacity is underestimated by the proposed models while the deviation from experimental data decreases as the temperature increases.

D. Structure. The structures of the proposed polarizable and nonpolarizable CO₂ models were investigated in terms of atom-atom radial distribution functions: $g_{OO}(r)$, $g_{OC}(r)$, and $g_{CC}(r)$. The structure of liquid CO₂ was experimentally studied by van Tricht et al. using neutron diffraction.⁵⁹ The

experimentally measured neutron-weighted pair correlation function $g_N(r)$ can be related to the atom–atom radial distribution functions using:

$$g_N(r) = 0.403g_{OO}(r) + 0.464g_{OC}(r) + 0.133g_{CC}(r) \quad (17)$$

Figure 9 shows the atom–atom radial distribution functions (bottom) of the polarizable model and neutron weighted pair

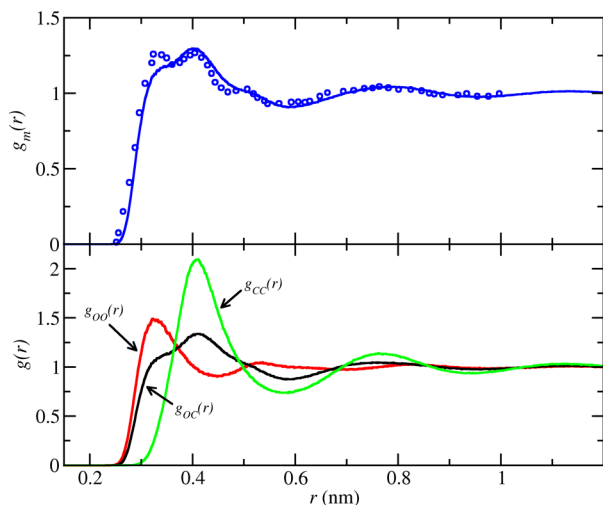


Figure 9. Atom–atom radial distribution functions of the polarizable CO₂ model (bottom) and neutron weighted pair correlation function $g_N(r)$ (top) at 239 K and 14.5 bar. Experimental pair correlation function is shown as blue circles,⁵⁹ and the simulation results from the polarizable model are shown as solid lines.

correlation function (top) at 239 K and 14.5 bar. The radial distribution function predicted by the nonpolarizable model is almost the same with that from the polarizable model, thus, not shown in Figure 9, but given in Supporting Information. In general, the structure of CO₂ is well represented by the proposed polarizable CO₂ model. It is noticed that $g_m(r)$ has two peaks at around 3.2 Å and 4 Å, respectively. The first peak is mainly due to $g_{OO}(r)$ and $g_{OC}(r)$, while the second peak is mainly resulted from $g_{CC}(r)$ and $g_{OC}(r)$. The proposed polarizable model underestimates the height of the first peak, while the prediction of second peak is consistent with experimental data in terms of both location and height.

E. Transport Properties. The self-diffusion coefficients of the proposed polarizable and nonpolarizable CO₂ models, for a wide range of temperature and pressure conditions, are shown in Figure 10. The two models are almost identical to each other and show a very good agreement with the experiment⁶⁰ with deviations of 5–6%. In Figure 11, the viscosity of the proposed models is plotted for temperatures ranging from 273 to 473 K and pressures 10 to 200 MPa. Again, both models show similar accuracy, with the nonpolarizable one being slightly more accurate. It is important to note here that the correlations of experimental data by NIST,³⁶ shown in Figure 11, fail to accurately predict the viscosities at low pressures, close to the vapor region (approximately 8 MPa). The inaccuracy is evident for the higher temperatures and for pressures under approximately 14 MPa, where we can see that the curves cross each other at various points. Our simulations for 373 and 473 K are done at 20 MPa, where no anomalies can be seen for

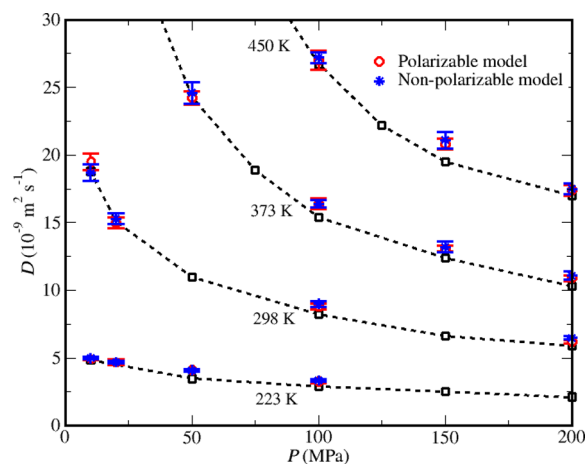


Figure 10. Self-diffusion coefficients of the proposed polarizable and nonpolarizable CO₂ models. Black open squares are the experimental data by Grob et al.,⁶⁰ and the dotted lines are to guide the eye. Open circles are simulation results from the polarizable model and stars are simulation results from the nonpolarizable model.

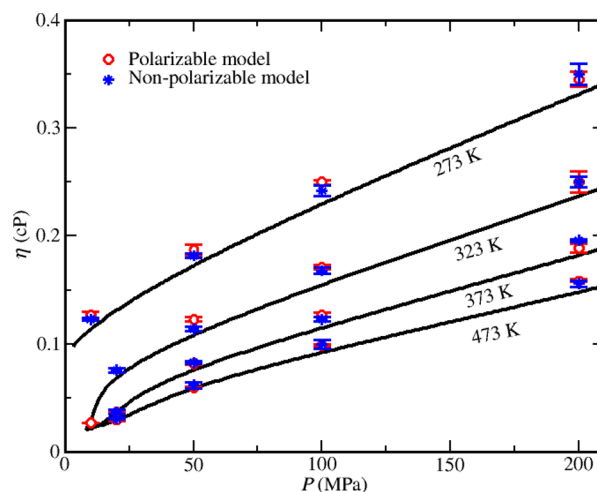


Figure 11. Viscosity of the proposed polarizable and nonpolarizable CO₂ models from 273 to 473 K. Solid black lines are experimental data from NIST,³⁶ open circles are simulation results from the polarizable model and stars are simulation results from the nonpolarizable model.

the experimental correlations and therefore it is safe to perform comparisons.

F. Comparisons with Prior Models. In Table 2, the proposed polarizable and nonpolarizable CO₂ models are compared with available nonpolarizable CO₂ models in terms of their average relative deviations (ARD%) from experimental data. These properties were calculated in the present work from the published force field parameters using the simulation methods described earlier. The performance of available nonpolarizable models are evaluated at the same conditions for the proposed models, and the details of the comparison can be found in the Supporting Information. The nonpolarizable model of Hasse et al.¹⁴ gives the best representation for saturated densities and vapor pressures, which is not surprising given that the model was optimized for these properties. The calculation of saturated densities and vapor pressures using the proposed polarizable and nonpolarizable models is slightly inferior but comparable to the model by Hasse et al.¹⁴ Although the Hasse model achieves remarkable accuracy for vapor

Table 2. Average Relative Deviation (ARD%) between Calculations Using CO₂ Models and Experimental Data^a

model	ρ_L	ρ_v	P_{sat}	ΔH	B_2	ρ_{fluid}	C_p	C_v	D	η
polarizable model	0.6	3.7	3.7	1.6	12.5	1.3	7.0	10.2	5.2	6.7
nonpolarizable model	0.9	2.4	3.2	1.9	12.4	1.0	8.3	10.6	6.3	5.7
TraPPE ¹⁰	0.9	5.3	3.0	6.4	12.5	1.8	7.6	10.2	5.5	8.4
Hasse ¹⁴	0.4	4.5	1.8	6.9	13.4	3.7	17.7	17.2		
EPM2 ⁹	1.0	10.6	12.9	2.6	17.1	1.9	27.0	11.1	12.4	1.7
Zhang-Duan ¹²	0.6	18.2	18.1	5.5	17.7	1.6	17.7	12.8	20.7	3.6

^aBold numbers indicate the smallest deviation for each property. $\text{ARD}\% = \sum_{i=1}^n \text{abs}[(A_{\text{sim},i} - A_{\text{exp},i})/A_{\text{exp},i}]/n$.

pressures, the representation of enthalpy of vaporization (ΔH) is less satisfactory with a deviation of 6.9% to experimental data, while the proposed polarizable and nonpolarizable models show much smaller deviations. The TraPPE model¹⁰ gives a reasonable representation for VLE properties, and it is comparable to the proposed models and the Hasse model.¹⁴ The EPM2 model⁹ shows larger deviations from experimental data for saturated vapor densities and vapor pressures, but its prediction for enthalpy of vaporization is satisfactory. It predicts viscosities very well, but has significantly lower accuracy for diffusion coefficients. The Zhang-Duan model,¹² which is essentially a variant of the TraPPE model, is inadequate to describe the VLE properties of CO₂. All the studied models systematically overestimate the second virial coefficient (B_2), and the proposed models give similar deviations as the TraPPE¹⁰ and Hasse¹⁴ models. The proposed polarizable and nonpolarizable models yield satisfactory overall agreement to experimental data for properties in liquid phase, including fluid density (ρ_{fluid}) and heat capacities (C_p , C_v). Also, they give excellent results for transport properties, with the polarizable model being the most accurate of all for diffusion coefficients. The Hasse model, though quite accurate for saturated densities, was found to be less accurate for the prediction of liquid densities especially at high temperatures and pressures, which indicates that a model optimized to VLE properties may not be necessarily suitable for simulations in supercritical region. The TraPPE model shows reasonable agreement with experimental measurement in one-phase fluid region. The EPM2⁹ and Zhang-Duan models¹² have similar performance and both show large deviations for prediction of heat capacities.

In summary, for VLE properties, the proposed polarizable and nonpolarizable models show comparable performance with the Hasse model,¹⁴ which is the most accurate potential model for VLE calculations. For liquid phase properties, the proposed polarizable and nonpolarizable models show better overall performance than previous available nonpolarizable models. The proposed polarizable and nonpolarizable models yield similar representation for most of the properties studied. The proposed polarizable model predicts a small but nonzero induced dipole moment (around 0.1 Debye) for liquid CO₂ at 250 K, and the induced dipole moment decreases as the temperature increases. The nonpolarizable models have zero induced dipole moment. Regarding simulation efficiency, the proposed nonpolarizable model has about 10% higher computational cost compared with the TraPPE and EPM2 models, which results from the Ewald summation of the Gaussian charges (versus point charges). The proposed polarizable model has a 5–10 times higher computational cost than the nonpolarizable model. This cost comes mainly from the energy minimization of the Drude particles and the computational overhead of the multiparticle move algorithm. Polarization contributes only 3–5% to the total energy of CO₂

at typical fluid conditions, because there is no strong electric field in pure CO₂. However, the effect of polarization is much stronger when mixing CO₂ with polar components, such as H₂O. Hence, the performance of the polarizable and nonpolarizable CO₂ model in fluid mixture could be very different and it would be worthy to use the more expensive polarizable model. The performance of the proposed polarizable model in mixture with H₂O will be investigated in our future work.

V. CONCLUSIONS

A Drude oscillator polarizable model and a Gaussian charge nonpolarizable model were developed for CO₂. The polarizable and nonpolarizable CO₂ models have rigid and linear geometry with carbon-oxygen bond length setting to the experimental values. The electrostatic interactions are represented by Gaussian charges, and the distribution of charges reproduces the experimental quadrupole moment. Using the Gaussian charge instead of point charge, the proposed polarizable model has great numerical stability against polarization catastrophe, and the polarization of CO₂ can be described with only three charge sites, which significantly reduces the computation cost. All three Gaussian charges take part in polarization by connecting to the molecular frame with harmonic springs. The van der Waals interactions of the proposed models are presented by Buckingham exp-6 potential, and the exp-6 potential parameters were adjusted to saturated vapor pressures, saturated vapor and liquid densities of CO₂ from 220 to 290 K, as well as the second virial coefficient at 220 K. The proposed models are able to accurately predict thermodynamic and transport properties of CO₂ over a wide range of conditions, and the polarizable and nonpolarizable models yield similar representation of pure CO₂ fluid properties. The second virial coefficients are slightly overestimated by the proposed models because the effect of many-body dispersion is not accounted in the models. The liquid densities are accurately predicted by the proposed models with relative deviation from experimental measurement typically smaller than 1%. The isobaric and isochoric heat capacities of new models are in reasonable agreement with experimental data, and the dramatic change of heat capacity with temperature is captured by the proposed models. For the structure of liquid CO₂, the predicted neutron weighted pair correlation functions by both the polarizable and nonpolarizable models are in close agreement with experimental data except that the first peak is slightly underpredicted by both models. With good representation of pure component properties, we expect the proposed models to be useful for the study of mixtures involving CO₂.

■ ASSOCIATED CONTENT

Supporting Information

The Supporting Information is available free of charge on the ACS Publications website at DOI: 10.1021/acs.jpcb.5b11701.

Tables with numerical values of the saturated vapor pressures, saturated vapor, and liquid densities, second virial coefficients, densities of homogeneous phase, heat capacities, diffusion coefficients, shear viscosities, and their corresponding statistical uncertainties (PDF).

AUTHOR INFORMATION

Corresponding Author

*E-mail: azp@princeton.edu

Notes

The authors declare no competing financial interest.

ACKNOWLEDGMENTS

We would like to thank Prof. Edward Maginn for access to early versions of the Cassandra codes. This publication was made possible by NPRP Grant No. 6-1157-2-471 from the Qatar National Research Fund (a member of Qatar Foundation). The statements made herein are solely the responsibility of the authors. Additional support was provided by the Office of Basic Energy Sciences, U.S. Department of Energy, under Award DE-SC0002128, and by the Carbon Mitigation Initiative at Princeton University. We are grateful to the High Performance Computing Center of Texas A&M University at Qatar for generous resource allocation.

REFERENCES

- (1) Solomon, S.; Plattner, G.-K.; Knutti, R.; Friedlingstein, P. Irreversible Climate Change Due to Carbon Dioxide Emissions. *Proc. Natl. Acad. Sci. U. S. A.* **2009**, *106*, 1704–1709.
- (2) Michael, K.; Golab, A.; Shulakova, V.; Ennis-King, J.; Allinson, G.; Sharma, S.; Aiken, T. Geological Storage of CO₂ in Saline Aquifers - A Review of the Experience from Existing Storage Operations. *Int. J. Greenhouse Gas Control* **2010**, *4*, 659–667.
- (3) Karplus, M.; McCammon, A. J. Molecular Dynamics Simulations of Biomolecules. *Nat. Struct. Biol.* **2002**, *9*, 646–652.
- (4) Maginn, E. J. Molecular Simulation of Ionic Liquids: Current Status and Future Opportunities. *J. Phys.: Condens. Matter* **2009**, *21*, 373101–17.
- (5) Panagiotopoulos, A. Z. Direct Determination of Fluid Phase Equilibria by Simulation in the Gibbs Ensemble: A Review. *Mol. Simul.* **1992**, *9*, 1–23.
- (6) Murthy, C. S.; Singer, K.; McDonald, I. R. Interaction Site Models for Carbon Dioxide. *Mol. Phys.* **1981**, *44*, 135–143.
- (7) Möller, D.; Fischer, J. Determination of An Effective Intermolecular Potential for Carbon Dioxide Using Vapour-Liquid Phase Equilibria from NpT + Test Particle Simulations. *Fluid Phase Equilib.* **1994**, *100*, 35–61.
- (8) Vrabec, J.; Stoll, J.; Hasse, H. A Set of Molecular Models for Symmetric Quadrupolar Fluids. *J. Phys. Chem. B* **2001**, *105*, 12126–12133.
- (9) Harris, J. G.; Yung, K. H. Carbon Dioxide's Liquid-Vapor Coexistence Curve And Critical Properties as Predicted by a Simple Molecular Model. *J. Phys. Chem.* **1995**, *99*, 12021–12024.
- (10) Potoff, J. J.; Siepmann, I. J. Vapor-Liquid Equilibria of Mixtures Containing Alkanes, Carbon Dioxide, and Nitrogen. *AIChE J.* **2001**, *47*, 1676–1682.
- (11) Potoff, J. J.; Errington, J. R.; Panagiotopoulos, A. Z. Molecular Simulation of Phase Equilibria for Mixtures of Polar and Non-Polar Components. *Mol. Phys.* **1999**, *97*, 1073–1083.
- (12) Zhang, Z.; Duan, Z. An Optimized Molecular Potential for Carbon Dioxide. *J. Chem. Phys.* **2005**, *122*, 214507–15.
- (13) Merker, T.; Vrabec, J.; Hasse, H. Comment on "An Optimized Potential for Carbon Dioxide" [*J. Chem. Phys.* **122**, 214507 (2005)]. *J. Chem. Phys.* **2008**, *129*, 087101–2.

(14) Merker, T.; Engin, C.; Vrabec, J.; Hasse, H. Molecular Model for Carbon Dioxide Optimized to Vapor-Liquid Equilibria. *J. Chem. Phys.* **2010**, *132*, 234512–7.

(15) Persson, R. A. X. Simple One-Center Model for Linear Molecules: Application to Carbon Dioxide. *J. Phys. Chem. B* **2011**, *115*, 10073–10078.

(16) Bock, S.; Bich, E.; Vogel, E. A New Intermolecular Potential Energy Surface for Carbon Dioxide from ab Initio Calculations. *Chem. Phys.* **2000**, *257*, 147–156.

(17) Bukowski, R.; Sadlej, J.; Jeziorski, B.; Jankowski, P.; Szalewicz, K.; Kucharski, S. A.; Williams, H. L.; Rice, B. M. Intermolecular Potential of Carbon Dioxide Dimer from Symmetry-Adapted Perturbation Theory. *J. Chem. Phys.* **1999**, *110*, 3785–3803.

(18) Bratschi, C.; Huber, H.; Searles, D. J. Non-Hamiltonian Molecular Dynamics Implementation of the Gibbs Ensemble Method. II. Molecular Liquid-Vapor Results for Carbon Dioxide. *J. Chem. Phys.* **2007**, *126*, 164105–8.

(19) Vlcek, L.; Chialvo, A. A.; Cole, D. R. Optimized Unlike-Pair Interactions for Water-Carbon Dioxide Mixtures Described by the SPCE and EPM2 Models. *J. Phys. Chem. B* **2011**, *115*, 8775–8784.

(20) Orozco, G. A.; Economou, I. G.; Panagiotopoulos, A. Z. Optimization of Intermolecular Potential Parameters for the CO₂/H₂O Mixture. *J. Phys. Chem. B* **2014**, *118*, 11504–11511.

(21) Persson, R. A. X. Gaussian Charge Polarizable Interaction Potential for Carbon Dioxide. *J. Chem. Phys.* **2011**, *134*, 034312–12.

(22) Axilrod, B. M.; Teller, E. Interaction of the van der Waals Type Between Three Atoms. *J. Chem. Phys.* **1943**, *11*, 299–300.

(23) Yu, K.; McDaniel, J. G.; Schmidt, J. R. Physically Motivated, Robust, ab Initio Force Fields for CO₂ and N₂. *J. Phys. Chem. B* **2011**, *115*, 10054–10063.

(24) Thole, B. T. Molecular Polarizabilities Calculated with a Modified Dipole Interaction. *Chem. Phys.* **1981**, *59*, 341–350.

(25) Kiss, P. T.; Baranyai, A. A Systematic Development of a Polarizable Potential of Water. *J. Chem. Phys.* **2013**, *138*, 204507–17.

(26) Kiss, P. T.; Baranyai, A. A New Polarizable Force Field for Alkali and Halide Ions. *J. Chem. Phys.* **2014**, *141*, 114501–15.

(27) Jiang, H.; Mester, Z.; Moulton, O. A.; Economou, I. G.; Panagiotopoulos, A. Z. Thermodynamic and Transport Properties of H₂O + NaCl from Polarizable Force Fields. *J. Chem. Theory Comput.* **2015**, *11*, 3802–3810.

(28) Graner, G.; Rossetti, C.; Bailly, D. The Carbon Dioxide Molecule A Test Case for the r_o , r_e and r_m Structures. *Mol. Phys.* **1986**, *58*, 627–636.

(29) Chialvo, A. A.; Cummings, P. T. Simple Transferable Intermolecular Potential for the Molecular Simulation of Water Over Wide Ranges of State Conditions. *Fluid Phase Equilib.* **1998**, *150*, 73–81.

(30) Kiss, P. T.; Sega, M.; Baranyai, A. Efficient Handling of Gaussian Charge Distributions: An Application to Polarizable Molecular Models. *J. Chem. Theory Comput.* **2014**, *10*, 5513–5519.

(31) Graham, C.; Imrie, D. A.; Raab, R. E. Measurement of the Electric Quadrupole Moments of CO₂, CO, N₂, Cl₂ and BF₃. *Mol. Phys.* **1998**, *93*, 49–56.

(32) Chialvo, A. A.; Vlcek, L. Ewald Summation Approach to Potential Models of Aqueous Electrolytes Involving Gaussian Charges and Induced Dipoles: Formal and Simulation Results. *J. Phys. Chem. B* **2014**, *118*, 13658–13670.

(33) Chialvo, A. A.; Moučka, F.; Vlcek, L.; Nezbeda, I. Vapor-Liquid Equilibrium and Polarization Behavior of the GCP Water Model: Gaussian Charge-on-Spring versus Dipole Self-Consistent Field Approaches to Induced Polarization. *J. Phys. Chem. B* **2015**, *119*, 5010–5019.

(34) Olney, T. N.; Cann, N. M.; Cooper, G.; Brion, C. E. Absolute Scale Determination for Photoabsorption Spectra and the Calculation of Molecular Properties Using Dipole Sum-Rules. *Chem. Phys.* **1997**, *223*, 59–98.

(35) Kong, C. L.; Chakrabarty, M. R. Combining Rules for Intermolecular Potential Parameters. III. Application to the Exp 6 Potential. *J. Phys. Chem.* **1973**, *77*, 2668–2670.

- (36) Linstrom, P. J.; Mallard, W. G. *NIST Chemistry WebBook, NIST Standard Reference Database Number 69*; National Institute of Standards and Technology, Gaithersburg MD; <http://webbook.nist.gov> (retrieved September 1, 2015).
- (37) Ungerer, P.; Boutin, A.; Fuchs, A. H. Direct Calculation of Bubble Points by Monte Carlo Simulation. *Mol. Phys.* **1999**, *97*, 523–539.
- (38) Eckl, B.; Vrabec, J.; Hasse, H. An Optimised Molecular Model for Ammonia. *Mol. Phys.* **2008**, *106*, 1039–1046.
- (39) Panagiotopoulos, A. Z. Direct Determination of Phase Coexistence Properties of Fluids by Monte Carlo Simulation in a New Ensemble. *Mol. Phys.* **1987**, *61*, 813–826.
- (40) Panagiotopoulos, A. Z.; Quirke, N.; Stapleton, M.; Tildesley, D. J. Phase Equilibria by Simulation in the Gibbs Ensemble. Alternative Derivation, Generalization and Application to Mixture and Membrane Equilibria. *Mol. Phys.* **1988**, *63*, 527–545.
- (41) Moučka, F.; Nezbeda, I.; Smith, W. R. Computationally Efficient Monte Carlo Simulations for Polarisable Models: Multi-Particle Move Method for Water and Aqueous Electrolytes. *Mol. Simul.* **2013**, *39*, 1125–1134.
- (42) Moučka, F.; Nezbeda, I.; Smith, W. R. Chemical Potentials, Activity Coefficients, and Solubility in Aqueous NaCl Solutions: Prediction by Polarizable Force Fields. *J. Chem. Theory Comput.* **2015**, *11*, 1756–1764.
- (43) Frenkel, D.; Smit, B. *Understanding Molecular Simulation*; Academic Press: San Diego, CA, 2002.
- (44) Baranyai, A.; Kiss, P. T. A Transferable Classical Potential for the Water Molecule. *J. Chem. Phys.* **2010**, *133*, 144109–10.
- (45) Siepmann, I. J. A. Method for the Direct Calculation of Chemical Potentials for Dense Chain Systems. *Mol. Phys.* **1990**, *70*, 1145–1158.
- (46) Shah, J. K.; Maginn, E. A General and Efficient Monte Carlo Method for Sampling Intramolecular Degrees of Freedom of Branched and Cyclic Molecules. *J. Chem. Phys.* **2011**, *135*, 134121–11.
- (47) Nosé, S. A. Molecular Dynamics Method for Simulations in the Canonical Ensemble. *Mol. Phys.* **1984**, *52*, 255–268.
- (48) Parrinello, M.; Rahman, A. Polymorphic Transitions in Single Crystals: A New Molecular Dynamics Method. *J. Appl. Phys.* **1981**, *52*, 7182–7190.
- (49) Kolafa, J. Time-Reversible Always Stable Predictor-Corrector Method for Molecular Dynamics of Polarizable Molecules. *J. Comput. Chem.* **2004**, *25*, 335–342.
- (50) Hess, B.; Kutzner, C.; van der Spoel, D.; Lindahl, E. GROMACS 4: Algorithms for Highly Efficient, Load-Balanced, and Scalable Molecular Simulation. *J. Chem. Theory Comput.* **2008**, *4*, 435–447.
- (51) Allen, M. P.; Tildesley, D. J. *Computer Simulation of Liquids*; Oxford University Press, 1987.
- (52) Einstein, A. Zur Elektrodynamik bewegter Körper. *Ann. Phys.* **1905**, *322*, 891.
- (53) Yeh, I. C.; Hummer, G. System-Size Dependence of Diffusion Coefficients and Viscosities from Molecular Dynamics Simulations with Periodic Boundary Conditions. *J. Phys. Chem. B* **2004**, *108*, 15873–15879.
- (54) Zeebe, R. E. On the Molecular Diffusion Coefficients of Dissolved CO₂, HCO₃⁻ and CO₃²⁻ and Their Dependence on Isotopic Mass. *Geochim. Cosmochim. Acta* **2011**, *75*, 2483–2498.
- (55) Moulτος, O. A.; Orozco, G. A.; Tsimpanogiannis, I. N.; Panagiotopoulos, A. Z.; Economou, I. G. Atomistic Molecular Dynamics Simulations of H₂O Diffusivity in Liquid and Supercritical CO₂. *Mol. Phys.* **2015**, *113*, 2805–2814.
- (56) Span, R.; Wagner, W. J. A New Equation of State for Carbon Dioxide Covering the Fluid Region from the Triple-Point Temperature to 1100 K at Pressures up to 800 MPa. *J. Phys. Chem. Ref. Data* **1996**, *25*, 1509–1596.
- (57) Yu, K.; Schmidt, J. R. Many-Body Effects are Essential in a Physically Motivated CO₂ Force Field. *J. Chem. Phys.* **2012**, *136*, 034503–7.
- (58) Herzberg, G. *Molecular Spectra and Molecular Structure*, 2nd ed.; Reitell Press: Davison, MI, 2008; Vol. 2.
- (59) van Tricht, J. B.; Fredrikze, H.; van der Laan, J. Neutron Diffraction Study of Liquid Carbon Dioxide at Two Thermodynamic States. *Mol. Phys.* **1984**, *52*, 115–127.
- (60) Groß, T.; Buchhauser, J.; Lüdemann, H. D. Self-Diffusion in Fluid Carbon Dioxide at High Pressures. *J. Chem. Phys.* **1998**, *109*, 4518–4522.